*energies*

MDPI

*Article*

# Analysis of the Dual Active Bridge-Based DC-DC Converter Topologies, High-Frequency Transformer, and Control Techniques

**Haris Ataullah [1], Taosif Iqbal [1], Ihsan Ullah Khalil [1], Usman Ali [1], Vojtech Blazek [2,*], Lukas Prokop [2] and Nasim Ullah [3,*]**

[1] Department of Electrical Engineering, College of Electrical and Mechanical Engineering (CEME), NUST, Islamabad 44000, Pakistan
[2] ENET Centre, VSB—Technical University of Ostrava, 708 00 Ostrava, Czech Republic
[3] Department of Electrical Engineering, College of Engineering, Taif University, Taif 21944, Saudi Arabia
* Correspondence: vojtech.blazek@vsb.cz (V.B.); nasimullah@tu.edu.sa (N.U.)

**Abstract:** A power conversion system needs high efficiency for modern-day applications. A DC–DC isolated bidirectional dual active bridge-based converter promises high efficiency and reliability. There are several converter topologies available in the market claiming to be the best of their type, so it is essential to choose from them based on the best possible result for operation in a variety of applications. As a result, this article examines the characteristics, functionality, and benefits of dual active bridge-based DC–DC converter topologies and the other members of the family, as well as their limits and future advances. A high-frequency transformer is also an important device that is popular due to high leakage inductance in dual active bridge (DAB) converters. Therefore, a detailed review is presented, and after critical analysis, minimized leakage inductance in the toroidal transformer is obtained using the ANSYS Maxwell platform. Furthermore, this work includes a comprehensive examination of the control approaches for DAB converters, which is important for selecting the most appropriate technique for a certain application. The outcome of ANSYS Maxwell is integrated with a DAB-based boost inverter in the MATLAB/Simulink environment, and the results are validated with the help of an experimental prototype.

**Keywords:** DAB converter; high-frequency transformer; isolated converters; control techniques; solid state transformer



**Citation:** Ataullah, H.; Iqbal, T.; Khalil, I.U.; Ali, U.; Blazek, V.; Prokop, L.; Ullah, N. Analysis of the Dual Active Bridge-Based DC-DC Converter Topologies, High-Frequency Transformer, and Control Techniques. *Energies* **2022**, *15*, 8944. https://doi.org/10.3390/en15238944

Academic Editors: Juan C. Vasquez, Gibran David Agundis Tinajero and Yajuan Guan

Received: 18 October 2022
Accepted: 23 November 2022
Published: 26 November 2022



## 1. Introduction

The dual active bridge (DAB) is a converter that is employed in solid-state transformers [1–3], applications like transportation [4,5], and renewable energy [6]. As shown in Figure 1, a DAB converter is composed of two inverters and a high-frequency transformer (HFT). This architecture enables input and output isolation while simultaneously reducing the volume. Furthermore, the voltage and power rating are chosen by design. The DAB converter is typically used as two DC–AC converters with square or quasi-square waveform voltage outputs and a phase shift between them. As illustrated in Figure 2, a bidirectional DAB converter interfaces high-voltage DC buses with low-voltage DC buses together in microgrids. A DAB can be used as either a buck or a boost and can transmit power in both directions. A bidirectional characteristic may be created in a traditional DAB by using an anti-parallel diode with a switching device (MOSFETs or IGBTs). This arrangement allows current to flow in both the forward and backward directions using controlled switching mechanisms. Because of its bidirectional capability, it decreases the system size, and enhances the performance and overall efficiency because it eliminates the need for two separate converters for forward and backward power flow.

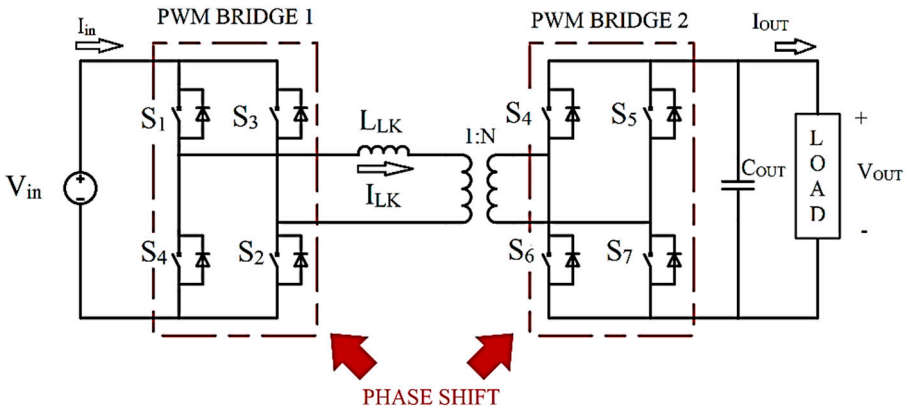


**Figure 1.** Topology of a dual active bridge (DAB) converter.

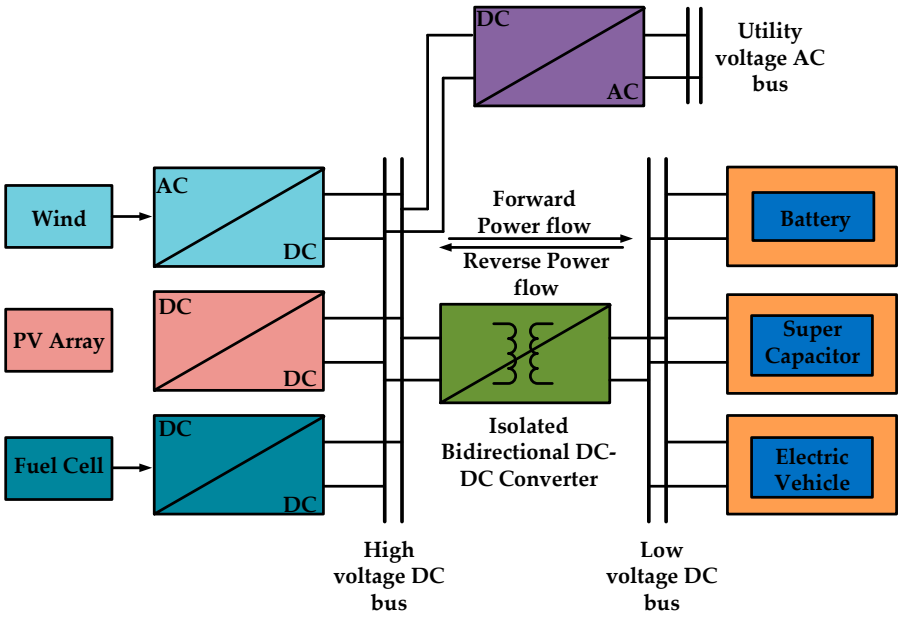


**Figure 2.** Microgrid with energy storage devices.

This topic has recently received a large amount of interest in academia, and many research papers on regulating strategies for DC–DC DAB converters have been written. A highly efficient DAB converter is required to manage the power flow in both directions, utilizing switching techniques for better and more efficient system performance. Because a DC–DC DAB converter contains two transformation phases (inverter stage and rectifier stage), an effective control mechanism is essential.

This study reviews and investigates DC–DC DAB converters and their control techniques; it is organized into families by explaining their individual kinds, as well as their pros and cons. The rest of this paper is organized in the following manner: Section 2 is about a high-frequency transformer being incorporated into a DAB converter and the study of the leakage inductance of toroidal transformers in an ANSYS Maxwell environment, Section 3 examines isolated converter topologies, Section 4 examines the control methodologies of DAB converters, and Section 5 presents the simulation results of a dual active bridge-based boost inverter followed up by prototype validation. Finally, Section 6 discusses the conclusion.

## 2. High-Frequency Transformer in DAB Boost Converter

Another significant consideration is the limitations of HFTs in DAB converters, predominantly governed by the materials utilized in their development [7]. Currently, the cores

used in HFTs are made of either ferrite or amorphous materials. Because of their high flux densities, cores made of amorphous materials allow for smaller inductors and transformers; hence, the HFT is reduced in size compared to a conventional line frequency transformer of same power [8]. However, in high-power applications above 100 KVA, commercial cores have size limitations; therefore, several cores have to be stacked to maintain the power. Also, the nominal frequency influences HFT power conversion, mostly because losses in the core increase as the nominal frequency rises [9]. In ref [10], the authors emphasize the parasitic capacitance of the HFT and its linkage with the other parts of the converter, where two major difficulties emerge, i.e., electromagnetic interference and resonance. If a natural resonance frequency is achieved, high harmonic currents can damage certain DAB components, and if electromagnetic interference is not minimized, converter control might suffer. As a result, the precise design of the HF transformer is important for the DAB converter's proper performance. This may be avoided by distributing the converter parts properly to avoid overheating the core. Finally, analyzing parasitic capacitances in the HFT helps to minimize difficulties caused by electromagnetic interference and resonance through the design of adequate control mechanisms. In HFT design, leakage inductance is very important. It slows the switching current at the device and prolongs the commutation time among output diodes. Furthermore, the energy stored in the leaking inductance causes voltage spikes in the switches. Measurements show a decrease in leakage inductance with increasing frequency. This is mostly because when frequency rises, the current distribution inside the conductor changes. At high frequencies, current concentrates on the edges of conductors, storing leakage energy in a small cross-sectional area. Because the total current remains constant, the leakage inductance is minimized at high frequencies.

The leakage inductance in the transformer is obtained by the proper design of a high-frequency toroidal transformer in ANSYS Maxwell, represented in Figure 3a, and as a result leakage inductance as a function of frequency is obtained as illustrated in Figure 3b. Design parameters of the HFT are given in Table 1 [11].

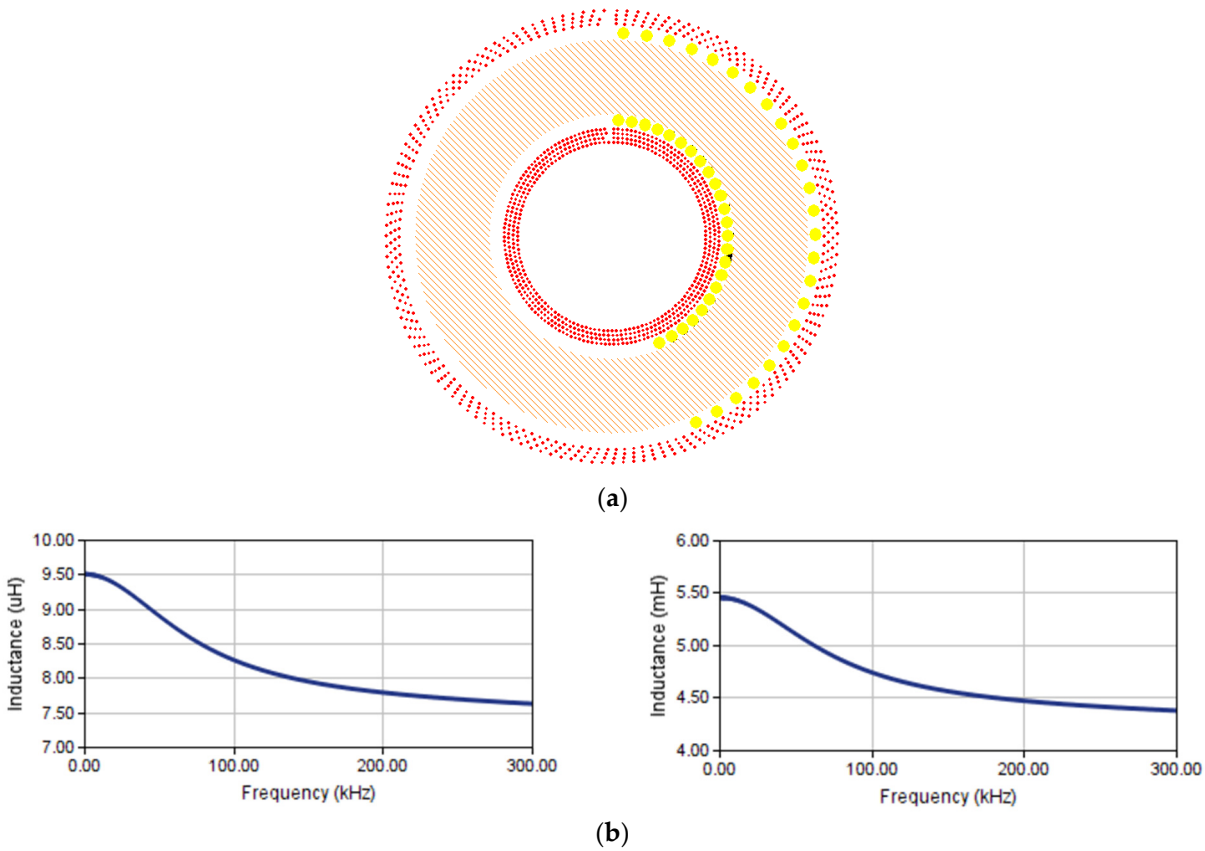


**Figure 3.** (**a**) Toroidal transformer in ANSYS Maxwell 2D environment. (**b**) Leakage inductance.

**Table 1.** Toroidal transformer dimensions [11].

| Dimensions and Characteristics | | Values |
|---|---|---|
| Outer diameter | $d_o$ | 80 mm |
| Inner diameter | $d_i$ | 50 mm |
| Core height | H | 20 mm |
| Effective length | $l_e$ | 197 mm |
| Effective cross-sectional area | $A_e$ | 295 $mm^2$ |

## 3. Topologies of DAB Converter

This section discusses various topologies of DAB converters. Isolation often occurs with a DC–AC–DC conversion sequence with two AC–DC stages. For galvanic insulation on the AC bus, coupled inductors or transformers are utilized for magnetic pairing. For safety and grounding considerations, isolation is necessary, particularly in applications requiring a fast rate of transformation to protect the LV side from the HV side. Separate structures in DC networks can supply various grounding platforms. In terms of similarities between DC–AC and AC–DC stages, isolated transformer converters are recognized as the dual active bridge (DAB) categories, irrespective of the bridge type.

### *3.1. Traditional 2L DAB*

The traditional 2L DAB consists of a two-level voltage source DC–DC converter on a moderate- or slightly high-frequency transformer's primary and secondary sides. Four switching devices are used for each bridge, as shown in Figure 4 [12]. Two complete bridges can generate two 50% square voltage waveforms by switching the complimentary switch pairs at a desired duty cycle. In a (DC) transmission, power is sent from the source to the load by the use of a phase shift. The magnitude and direction of power can be observed by the magnitude and sign of the phase-shifted angle [13]. Due to the ease of soft switching control and low inertia, modulation control is used in 2L DAB converters. However, high circulating current is produced if the amplitudes of both H-bridges on both sides of a transformer are not similar. This result is due to the turns ratio of the HFT i.e., $(V_1/nV_2)$, where n is the turns ratio. Therefore, the circulating current will be high, which will result in the RMS and peak current. The inner phase-shift ratio expands the ZVS range and reduces the circulating power and current [13]. Various modulation strategies have been studied in detail in the literature review, like extended-phase-shift modulation (EPS) [14], double-phase-shift modulation (DPS) [15], and triple-phase-shift modulation (TPS) [13]. In EPS, like single-phase-shift modulation (SPS), the bridge on the primary side of the HFT is switched, and the switches on the secondary side of the high-frequency transformer change their states based on inner phase-shift operation [13], enabling the primary bridge to generate 3L output AC voltage and the secondary bridge to generate a 2L square wave. The outer phase shift is responsible for the magnitude of power flow and its direction, while the inner phase shift helps in ZVS range expansion while reducing the circulating current [13]. Similarly, in DPS, the switches in the complementary fashion are switched in both the bridges using a similar inner phase-shift ratio, therefore generating 3L AC voltage at the output [13]. When compared to the SPS method, using this modulation method ensures an expanded range of ZVS, reductions in both current stress and output capacitance, and easy implementation of deadband compensation under specific conditions [16]. In high-power applications, the DAB converter is preferred over other topologies because it can achieve zero-voltage switching (ZVS), thus reducing switching losses in semiconductor devices and helping to achieve high efficiency. Similarly, maximum transfer of power depends on the leakage inductance of a transformer, hence the elimination of the resonant capacitor [17]. High dv/dt stress on the isolation of the AC link is the major drawback of a DAB. The current spike may be generated with a SiC IGBT/MOSFET switching current ring [12]. In addition, snubber circuits may also be employed to various circuits to produce static and dynamic voltage-sharing balances to decrease excessive losses [18,19].

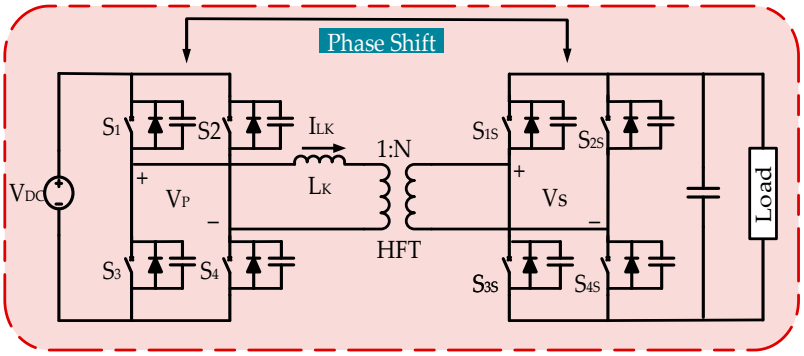


**Figure 4.** The traditional DAB converter.

### *3.2. Three-Phase DAB*

The three-phase DAB is the modified version of the typical 2L converter comprising two full three-phase bridges. On the primary side of the high-frequency transformer (HFT), a three-phase inverter is connected for the conversion of DC to AC, while a three-phase inverter rectifier is connected on the secondary side of the HFT. It delivers the six-step waveform of AC voltage across the center winding of the transformer. The six-step mode results in a zero-voltage turn-on for inductive loads, and an important decrease of turn-off loss is achieved by the linked snubber capacitors between the power electronic devices [19].

The three-phase DAB is advantageous in high-power applications compared to some other options due to the following reasons: a major amount of transfer of power because of a low RMS current of the transformer, power due to high density, element stress, modularity, and less ripples in the current and minor filter capacitor [20,21]. With a large phase shift, the RMS currents can be increased in single-phase modulation, thus resulting in significant conduction losses. The conversion of non-unity voltage also leads to high circulation of current and restricted switching range [22]. This can influence the efficiency and stability of light loads within a wide range of voltages. The foregoing problems cannot be handled entirely by various sophisticated modulation methods. The only solution to this problem is the resonant system for low and medium power in three phases and the resonant immittance system in three phases for high power [20].

### *3.3. Multilevel DAB*

To increase the performance of the conventional DAB converter, the multilevel (ML) single-phase or three-phase DAB converter is essential. The voltage limitation of power semiconductor switches can be achieved with the capability to supply more than two voltage levels. It is worth noting that ABB has utilized a multilevel three-stage converter topology for a 1.2 MVA, 15 kV SST prototype [23]. Compared to the 2L DAB, the ML DAB converter has small dv/dt stresses, resulting in improved efficiency of the overall system and a high power density [16]. Such converters therefore enable the operation of LV-specific devices using certain methods, such as minimizing switching and conduction loss and improving the fault-tolerant capacity [11]. The voltage stress of a switch can be reduced to half the terminal voltage by means of a good control scheme [24]. The fault-tolerant capacity means that the system can still operate with reduced performance under the fault condition. Because flying capacitors are used in most multilevel DC–DC converters, their voltage can be used as a diagnostic variable for short-circuit fault diagnosis/detection [21]. A further aspect which causes fewer magnetic losses in converters is that the total harmonic distortion in voltage and current waveforms is reduced [11,25]. The neutral point clamp (NPC) diode is efficient for high energy density in medium- and high-voltage applications [26]. Furthermore, 3L NPC legs can be placed on either side of the DAB [27,28]. In running ZVS, an evaluation of modulation systems and components was introduced between the five-level DAB and the 3L DAB [28]. The 3L NPC DAB is beneficial to the high-voltage waveform of the transformer, which reduces switching and conduction losses [29]. Each

switch's voltage stress is also lowered by 50% of the port voltage on both bridges. A few research articles on multilevel voltage balancing are available, and the solutions offered are all about high switching for fundamental frequency. This technique is not appropriate for NPC DAB converters. Another technique for voltage balancing is the vector adjustment of active bridges. This is based on detecting the voltage imbalance and the direction of power flow. Another NPC technology is a blocking capacitor used in active bridges and utilizing asymmetric voltage pulses on the sides of the transformer [30]. During the zero-voltage vector period, the optimum switching time allocated to the internal switching pairs will be changed to permit the charging of capacitors, irrespective of the power flow direction [31]. Nevertheless, a significant problem for the multilevel NPC DAB is the imbalanced voltage of the capacitors connected in series. This is because one phase among all is connected to a neutral point [32–34]. While [31] delivers an appropriate control and modulation mechanism and offers a suitable equilibrium in a variety of levels of voltage and broad-based operating circumstances, complexity in control and a large quantity of semiconductor devices correlate with ML DABs [11].

### *3.4. Cascaded Multi-DAB*

Several low-power and low-voltage converters can be linked in sequence to construct a medium-voltage cascaded multi-DAB. The required voltage can be achieved by connecting low-voltage cells in series. A transformer is used to give galvanic isolation to every individual cell for an isolated DC input. Topologies of this type do not need transformers with low frequency. This converter is therefore appropriate for applications like PVs, fuel cells, and batteries with independent DC sources [35,36]. In the case of high power density, cascaded DABs may work at higher frequencies because of low rating of the cells, which leads to low voltage stress and small filters [36]. Due to a fraction of the net power being distributed by every cell, the current device's rating decreases [36]. The input/output side can be connected in series or in parallel. For high-power and high-voltage applications [37], parallel input series output (PISO) systems are appropriate and can lower the number of devices if a diode rectification is swapped for full bridge converters at the output of the DAB [38]. The series input and series output (SISO) converter consisting of complete bridge modules is shown in Figure 5. Each model has two H bridges, having four switches at the primary and secondary sides of the high-frequency transformer and a high-frequency transformer in the center [38]. In the absence of a quick fault current [37], it provides adequate performance in fault situations. The primary disadvantages of this arrangement are the excessive numbers of transformers and switches, leading to a complex control mechanism and significant driving losses.

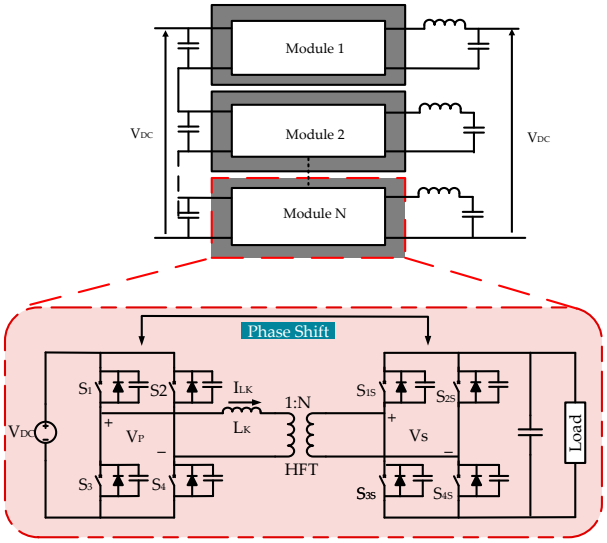


**Figure 5.** Cascaded Multi-DABs.

### *3.5. Modular Multilevel DAB (MMC DAB)*

Figure 6 illustrates structure of the MMC DAB converter constructed by two MMCs with a single center-tapped transformer. An AC voltage source can be imitated by one of the MMCs; the other, as the current source, may be controlled [39]. The MMC DAB converter can be constructed with more than two phases, as indicated by the tri-phase MMC in [37]; therefore, this results in regulation of the same submodule (SMs) in every arm of the MMC, and the AC voltage is created. SMs may be implemented by several sorts of bridges for a variety of functions. The most used types are the half-bridge submodule (HBSM) for unipolar voltages and the full-bridge submodule (FBSM) for better DC fault-handling of bipolar voltages [39]. In the case of a change in input, the output voltage and operating power have little effect on MMC efficiency. Due to the multiple-switch functionality that may exist in the MMC, it can be possible to restrict the working frequency of the transformer [40] and to have a high total device rating (TDR) [39]. This approach nevertheless increases the medium-frequency operation, which lowers the size and weight of the passive components. The management of these multi-modular converters results in the control of the transfer of power using the transformer sides of two phase-shifted waveforms [39]. Various modulation methods include quasi-2L (Q2L), quasi-3L (Q3L), and sinusoidal, which contribute to optimal functionality of the converter [39]. Creating a transformer design that works for quarterly waveform operation is a difficult task at medium frequency [39]. The face-to-face assembly of two MMCs allows bidirectional tasks, but the sizes, costs, and losses of the converter are considerably high.

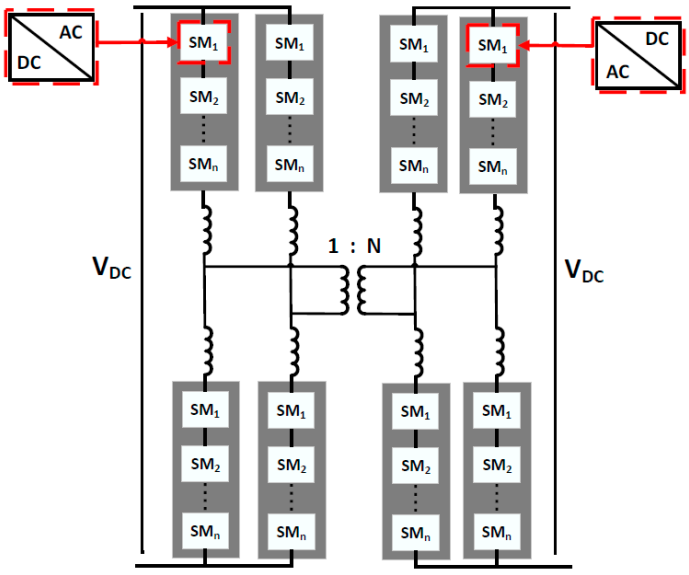


**Figure 6.** MMC DAB.

Another example of a hybrid converter created by ABB [41] is the combination of a two-level converter (TLC) and a multi-modular converter (MMC), which results in a two-level multi-modular converter (TLC–MMC) [40,42]. It may be used for a broad variety of levels of power and voltage. The small rating of such a device and less switching losses in the semiconductor device guarantee efficiency. The approach of direct modulation produces sixth-order voltage and current oscillations. Indirect modulation can solve this problem. Indirect modulation can accomplish the voltage-balancing of the MMC by injecting circulating currents into the MMC to balance the voltage by the circulation of power between arms. Voltage is balanced by injecting circulating DC current into the three-phase leg. Each leg in the MMC has its lower and upper arms and a sinusoidal circulating current which helps in balancing the voltage between them. Based on the MMC DAB, both DAB and MMC converters may benefit from small passive components and soft switching, ensuring a high density of output and high efficiency [43].

However, it is necessary to have two complete MMC converters, and the MMC DAB contains double the semiconductor components. This leads to much loss of conduction and cost. The hybrid MMC settings can fix this problem. Despite the benefits of the TLC–MMC, the capacitor balancing of the arm conductor requires a special technique of balance control [41]. A high number of capacitor submodules is also needed, and three single-phase legs are integrated [44]. All the topologies including its pros and cons with its applications are summarized in Table 2.

**Table 2.** Characteristics of DAB converters [22].

| Ref. No. | Converters | Pros | Cons | Applications | Voltage Ratio |
|---|---|---|---|---|---|
| [20] | Three-phase DAB | • Power transfer is high.<br>• Value of filter capacitor is small. | • In single-phase modulation, induction losses are high.<br>• Circulating current is high. | • Interconnection of DC grids.<br>• Solar applications. | It is based on series-connected switches and DC step ratio. |
| [27,28] | Multilevel DAB | • Low dv/dt stress.<br>• Low THD.<br>• Lower total device rating (TDR).<br>• Operations are performed under high frequency. | • Unbalancing of capacitor voltage.<br>• Complex control design<br>• Number of switches is high | • Solar applications.<br>• DC transformers. | Voltage ratio is high. |
| [36] | Cascaded Multilevel DAB | • Voltage stress is less.<br>• Filter components requirement is less. | • Complex control design<br>• Increased amount of components.<br>• Increased conduction. losses. | • Offshore wind.<br>• Solar applications.<br>• Solid state transformer. | It depends on the amount and connection of modules. |
| [38] | Modular Multilevel DAB | • Controlled dv/dt.<br>• Small passive elements.<br>• Soft switching. | • Large number of submodules.<br>• Complex control for balanced voltage. | • Interconnection with DC grid.<br>• Offshore wind.<br>• DC transformer. | Module connection-dependent. |
| [20,45] | Resonant DAB | • High frequency.<br>• Soft switching<br>• Increased efficiency. | • Increased volume due to large number of components. | • Electric vehicles. | Medium-High. |
| [46] | 2L DAB | • Device rating is low.<br>• Capacitor value is small. | • High dv/dt stress on the AC link insulation. | • Electric vehicles.<br>• Solar. | It depends on the connection of the switch and DC step ratio. |

### *3.6. Isolated Resonant DAB*

In the range of the turning on and off rotation at peak current, the DAB converter has restrictions. This affects the efficiency and component sizes in the management of high-current stress effects. Addressing the challenge, the DAB converter is supplemented with a series of resonant tanks to guarantee high control flexibility in terms of efficiency [45,47]. The resonant LLC converter was executed in [45], having a resonant inductor, capacitor, and shunt inductor connected in series, by analogy to the standard DAB DC converter, in the magnetic transformer inductance [45,47]. Leakage inductance has an influence with high turning ratios on the transformer, which produces higher overshoots through the semiconductors. The addition of leakage inductance can be useful in decreasing losses in the resonant tanks. In [48], a resonant CLLC DAB converter is proposed with reduced switching losses and improved power supply capabilities of the transformer. It is preferable to use a resonance tank to increase the voltage along with more powerful soft switching [46,49,50]. Nevertheless, the DAB converters in series have some disadvantages

that lead to huge sizes, reduced cost-effectiveness, and a substantial amount of constant frequency off losses [48,51].

## 4. Control Methodologies Used in DAB Converter

Based on various variants and topologies, DAB converters have tremendous control methods [52]. Here we study various techniques to gain an idea of how the control of a DAB converter is implemented. Table 3 summarizes the control techniques applied to DAB converters.

**Table 3.** Review of control techniques for DAB converters [8].

| Control Techniques | % |
|---|---|
| PID | 34.4 |
| Sliding mode control | 21.9 |
| Model predictive control | 9.4 |
| Fuzzy logic control | 6.3 |

### *4.1. Phase-Shift Modulation*

Phase-shift modulation control has a history from the primary stage to up to the present [50] for being a component of strict growth with a view toward improving efficiency in the techniques and means of obtaining an effective DAB converter. The pros and cons of the systems indicated in Table 4 are also included. The modern, unified phase-shift modulation technology is flexible and integrates all prior techniques.

### *4.2. System Variables Control*

The following various control and modulation techniques are part of control stages for DAB converter. Usually, control factors such as input DC voltages and output load current can be considered. These variables are used to achieve the ideal values such as the intended transmission of power under different situations. According to the characteristics of these factors, they consist of either a DC value or the components of the switching frequency. In certain situations, authors use variables like high-frequency link variables, including inverter voltage and inductor current on both sides of a high-frequency transformer. However, the technique applied for control is rather hard to perform practically, as the situation requires more-powerful voltage sensors and a high-bandwidth current, and the results of the converter do not change much.

The following control techniques are based on a slowly varied parameter in the concerned literature.

- Direct control of power in the DAB [53].
- Control for lowest current stress [54].
- Modulation of zero circulating current [55].
- Control for virtual direct power [56].
- Control for reactive power minimization [57].

**Table 4.** Phase-shift modulation strategies [58].

| Ref. No | Modulation Technique | Pros | Cons |
|---|---|---|---|
| [59] | SPS | 1. Soft switching control is easy.<br>2. System is more dynamic. | 1. Large circulating current.<br>2. Zero-voltage switching. |
| [60] | EPS | 1. Improved efficiency.<br>2. Improvement in zero-voltage switching. | 1. Circulating currents do exist. |
| [61] | DPS | 1. Easier to implement.<br>2. Excellent dynamic performance. | 1. Dynamics and stability increases make the system more complex. |
| [62] | TPS | 1. Broad range of inputs results in great dynamic performance for load changes. | 1. Control complexity.<br>2. Operating states vary for buck/boost approach. |

The control goals based on system variables are clearly shown in Figure 7.

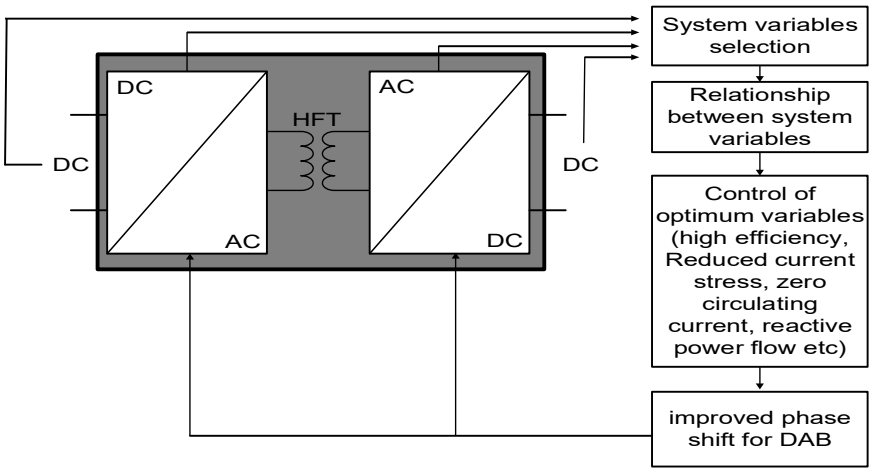


**Figure 7.** Detailed representation of DAB converter control techniques.

*4.3. Proportional–Integral–Derivative Control*

The easiest and simplest-to-implement control approach is basic PID control. It has a great control dynamic with zero stability errors, very rapid responses, and improved stability as the main solution to the construction of a control algorithm.

In [63], a hybrid PI controller based on a second-order Taylor series estimator for the offset between the pulse-width modulation of both bridges and an auxiliary PI control is implemented. The switches are controlled using the single phase-shift (SPS) approach, and the control strategy is developed using an averaged model. Last but not least, the findings relied on simulations and included no efficiency analysis.

The study given in [64] in 2012 offered two control approaches depending on a Fourier series model that aimed to improve the conventional PI control model. The original setup included a PI controller for output voltage regulation and a feedforward control approach for inverter power ripple control. Both control strategies used the output voltage and the leakage current as control variables and decoupled into Fourier series for easier manipulation. The second solution is a proportional–integral–resonant (PI-R) control algorithm, in which the PI part regulates the output voltage, and the resonant element adjusts for the ripple produced by voltage inversion. Using Bode diagrams, both the new and standard PI solutions were simulated in order to evaluate the control results.

In [65], a boost and DAB converter integrated with a PV and battery, respectively, along with a PI controller are compared and simulated in MATLAB/Simulink. The goal is to model the system with its control implementation without any experimental verification

In [66], the authors recommend DAB converters for applications like electric vehicles, allowing for the reduction of both electrical and control restrictions via the use of an appropriate control scheme. The suggested PI control system regulates the output voltage, and an experimental hardware prototype based on FPGA and a battery emulator achieved a 95.6% efficiency.

In [67], a PV and battery-based DAB converter is proposed using proportional resonant control, and a microgrid is integrated into the output. The author models each system, i.e., PV and battery along the microgrid, using the subsystem block in MATLAB/SIMULINK.

The PID controller's generic block design is depicted in Figure 8. In a conventional bidirectional DC–DC converter, a PWM is utilized to produce a pulse triggered by a switch. Because the fire angle is adjusted, a large variation in output voltage is detected due to a slight difference in input voltage. To solve this problem, the PID controller is proposed [68]. The PID working paradigm is described in [69,70]. Although there was variation in the input voltage, the output voltage remained the same because the converter output voltage was correlated with the appropriate set of values, and a triggered signal was sent to a switch

for the required output voltage. Similarly, in [71], a comparison of the stability of the output voltage of PID and PI controllers is made for bidirectional converters of electric cars. With the PI control technique, less fluctuation is noticed in the output voltage for varied input supply voltages. There is always a balance between the overshoot and stability of output voltages when selecting a PID or PI controller. PID controllers are very reliable, dynamic, and suited for several control problems. However, in the face of uncertainty and great trouble, they do not have the required flexibility. There are numerous applications in which their efficiency is quite poor, particularly if there is nonlinearity in the system.

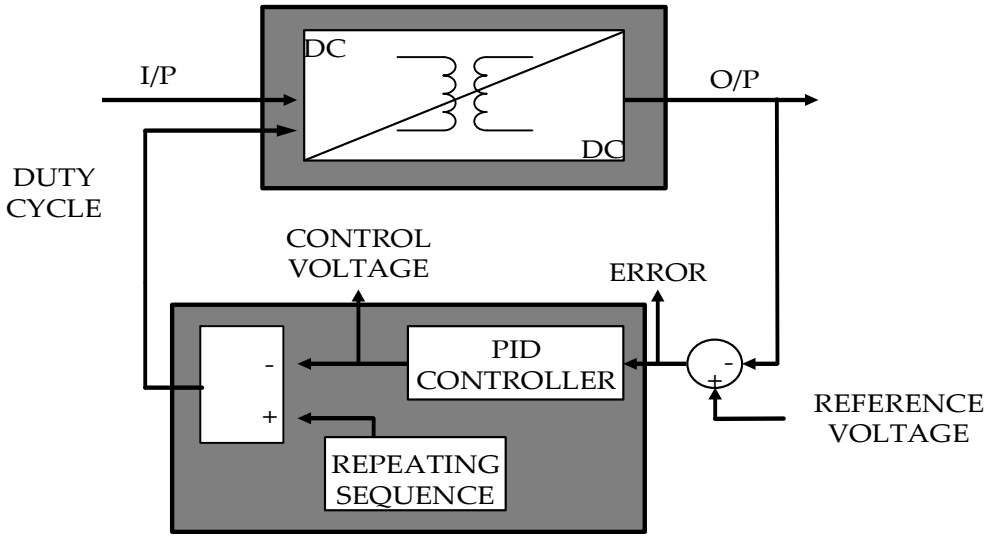


**Figure 8.** Block diagram of PID control.

*4.4. Sliding Mode Control*

The dynamic equation of the converter is not linear because of nonlinear components in various configurations of the two-way DC converters. One approach to the construction of the control algorithm is to linearize the system using various linearization methods. This technique does not, however, reflect the precise model, as it is based on hypotheses and assumptions. Thus, it is better to utilize nonlinear control methods to regulate bidirectional DC–DC converters to achieve a stable and dynamic system that can answer to external disturbances. Sliding mode control is the common nonlinear technique due to its fast, dynamic response, parameter change robustness, and low external sensitivity [72]. The generic block diagram for sliding mode control is shown in Figure 9. In [73], a sliding mode is suggested for a DC–DC bidirectional coupling inductor converter. The sliding-mode technology suggested tracked the high-performance reference DC voltage on the high side and proved its robustness against disturbance. In [74], a bidirectional DC converter is investigated using sliding mode control. Comparison between PI and sliding mode control is carried out regarding load disturbances and parameter changes.

In [75], a DAB converter using a sliding mode controller and fuzzy logic control is proposed. The major objective was to regulate the output voltage ($V_{out}$) and leakage inductor current ($i_{LK}$). The results demonstrate that the response of the fuzzy logic controller is better than that of the sliding mode controller (SMC) due to smooth battery charging and discharging. The simulation platform used was MATLAB/SIMULINK and Proteus.

In [76], an SMC used in DAB converter with a DC load is proposed. Dynamic modelling of a converter is used to decay the AC operation of a converter by using a Fourier series. SMC and PI, incorporating perturbations, were compared for the validation of a model.

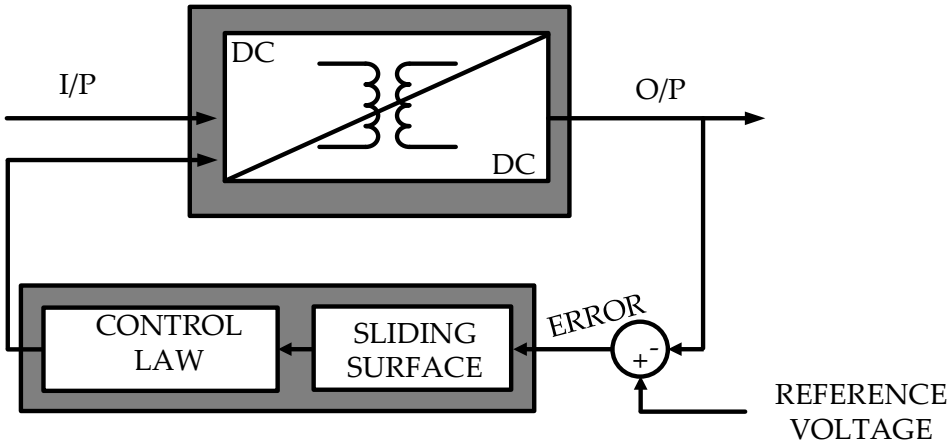


**Figure 9.** Representation of sliding mode control.

In [77], the authors discussed a hierarchal sliding mode controller (HSMC) to operate dual DAB converters in parallel at the input but in series at the output (IPOS). The controller within this recent study was focused on the $i_{LK}$ and $V_{out}$ of each converter, allowing the control system to correct for the impacts of power mismatching among the converters. This method was evaluated through an experiment by perturbing converters with a distinct profile to confirm the performance of the controller.

The sliding mode control approach is robust and has a good dynamic response. However, certain restrictions are also present, as correct parameters and state data are needed. In addition, undesired oscillations within the final frequency and amplitude might occur in the sliding mode control approach. These unwanted oscillations are called 'chattering' [71]. A sliding control method is provided in [78] to decrease this chattering behavior. Although external disruptions occur, great robustness may be generated, and the system becomes stable when system oscillations are minimized.

### *4.5. Model Predictive Control*

The prevalent and emerging algorithm for energy conversion systems and power electronics is model predictive control. Figure 10 illustrates the block representation of the predictive model. This model is the most appealing control technique compared to other traditional approaches due to its very quick dynamic response and its fast-tracking characteristics.

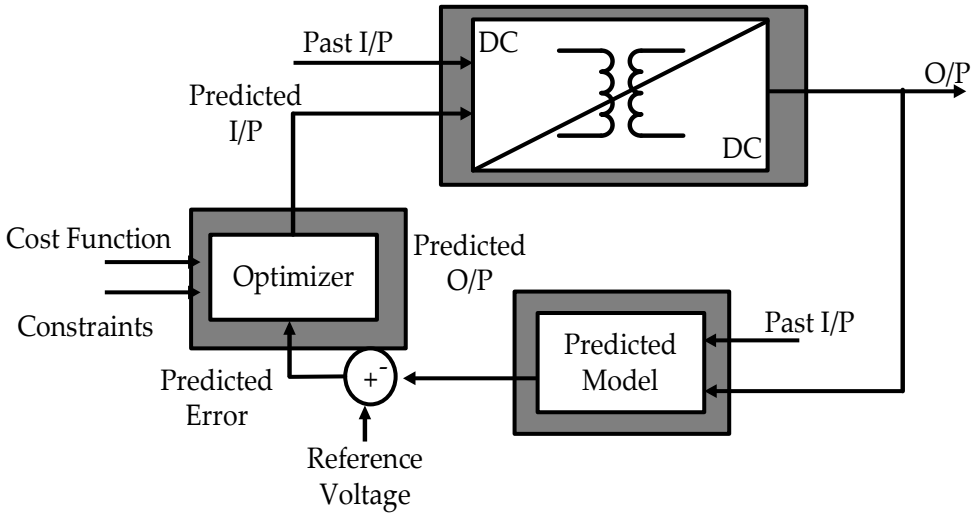


**Figure 10.** Block diagram of model predictive control.

A medium-voltage direct-current (MVDC) control system for ship power systems is proposed in [78,79]. A linear quadratic internal (LQI) control is utilized to create a linear model predictive controller (MPC) for such a solution. The findings suggest that the reactions to disturbances are adequate. In ref [80], the authors proposed an MPC including current stress optimization (CSO) for a dual DAB linked in parallel at the output ports. The solution begin by using a standard voltage-mode control (VMC) technique before proceeding to a CSO; lastly, an integration of CSO and MPC is suggested. This article states that the CSO–MPC can manage power in both converters for various operating ranges without any overshoot and while improving load security.

In [81], the authors proposed a moving discrete-time predictive model and adaptive control technique to enhance the converter's efficiency by managing the output voltage. Such a hybrid approach outperformed a traditional PI controller in terms of robustness and efficiency, but at a greater computational cost, necessitating an expensive implementation.

A great number of computations are needed for this approach, but today it is easy to apply using a rapid and powerful microprocessor, and it is utilized in fuel cell/battery/super capacitor energy management [82]. In [83] bidirectional DC–DC converters are conceived using a model-based control algorithm, whereby a 2.5 KW model for a double-phase shift (DPS) combined with PWM-based control approach and predictive method is experimentally tested for efficiency. The converter efficiency was found to be 89.56% using the double-phase shift technique, while the converter efficiency improved to 92.52% with the predictive method because of the zero-phase shift of the model-predictive method and the unity factor between the voltages and the high-frequency transformation currents, which decreases the total reactive power of the converter.

Different control techniques used in DAB converters are responsible for efficiency improvement. Figure 11 summarizes the control techniques for DAB converters based on different energy sources.

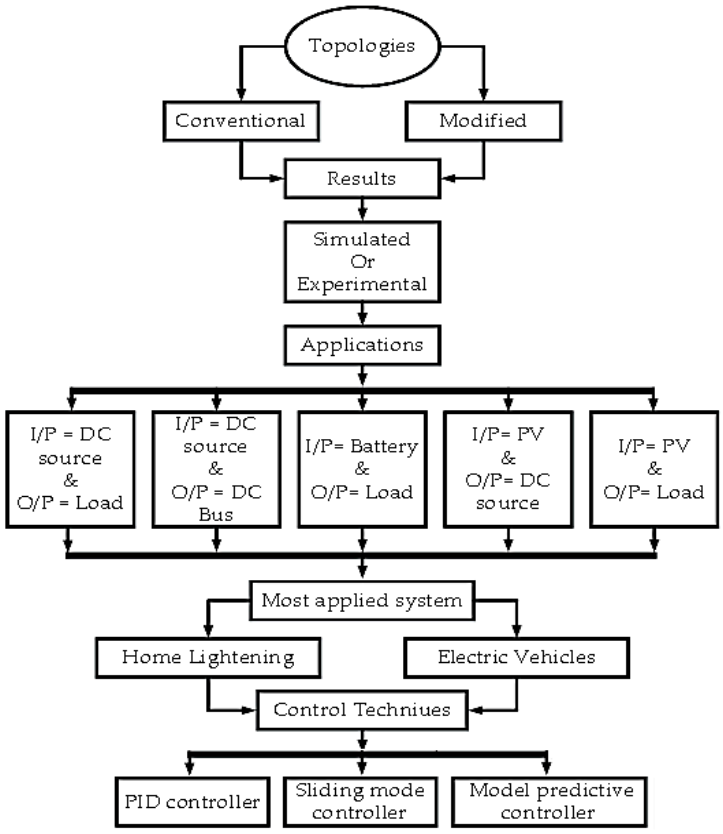


**Figure 11.** Summary of various control techniques.

## 5. Simulation Results

Figure 12 depicts an essential topology of the dual active bridge-based boost inverter discussed below. The outcomes of these simulations are shown in Figures 13–16. In Table 5, the simulation and experimental parameters that were employed are shown. Assuming an input voltage of $V_{in}$ = 12 V and an output voltage of $V_{out}$ = 285.6 V, with a modulation index of $MI$ = 0.85 and a load resistance of $R_L$ = 100, the DC voltage is maintained at a constant value. Table 6 provides the calculated values.

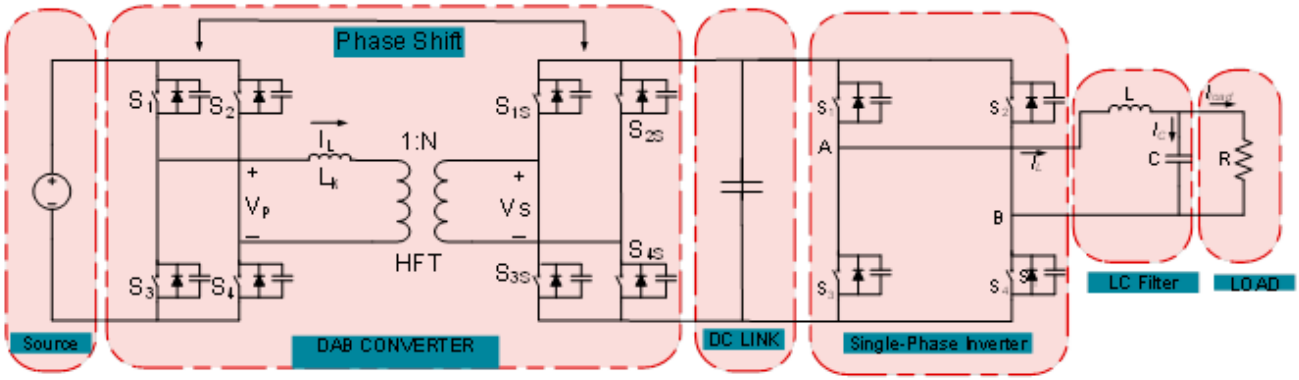


**Figure 12.** Dual active bridge-based boost inverter topology.

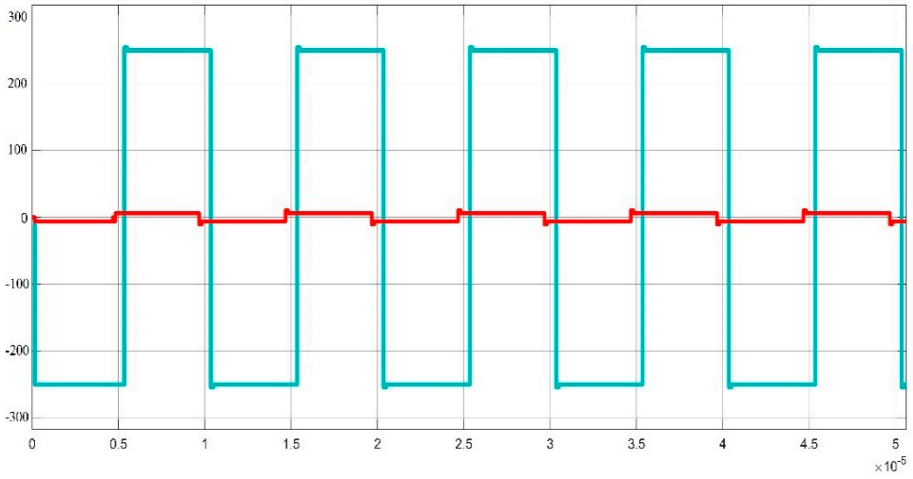


**Figure 13.** Transformer primary Voltage = 13V (red) and secondary voltage = 270V (Blue).

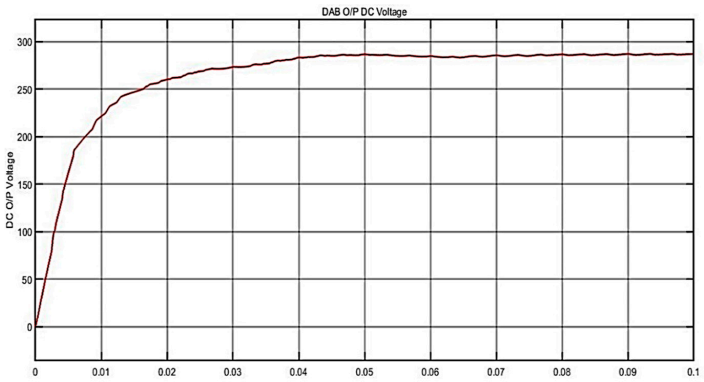


**Figure 14.** Output voltage waveform.

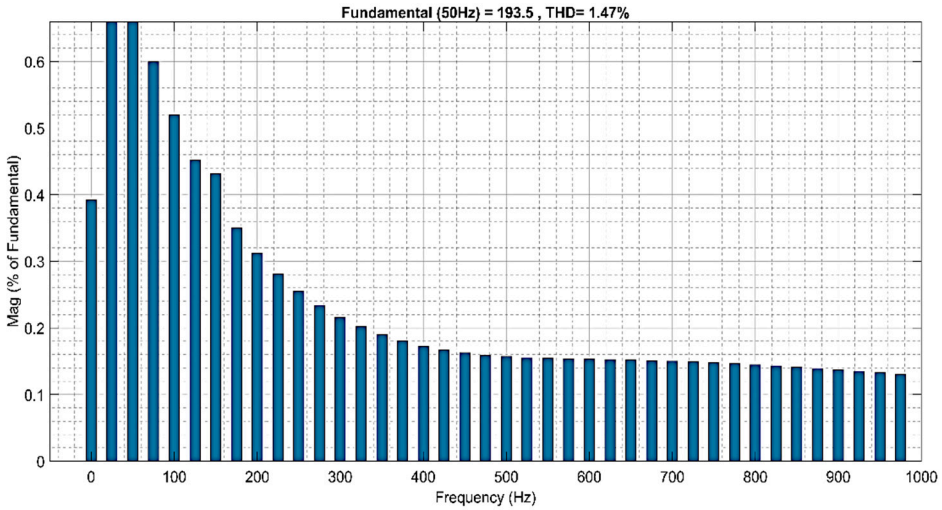


**Figure 15.** Simulated THD of the output voltage under SPWM.

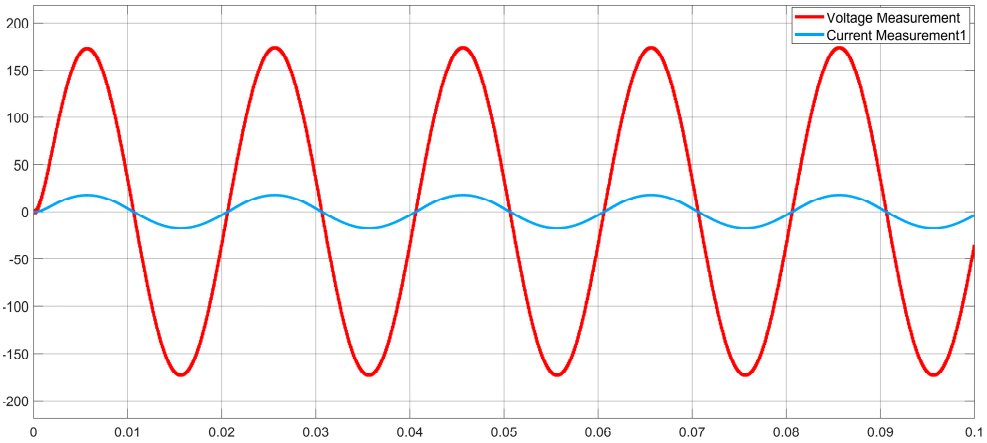


**Figure 16.** AC output of DAB-based boost inverter.

**Table 5.** Proposed scheme parameters [10].

| Circuit Parameters | | Values |
|---|---|---|
| Input Voltage | $V_{in}$ | 12 V (DC) |
| Output Voltage (DAB) | $V_{out}$ | 294 V (DC) |
| Turns Ratio | $N_P$:$N_S$ | 1:25 |
| Switching Frequency | $f_{S(VSI)}$ | 10 kHz |
| Switching Frequency | $f_{S(DAB)}$ | 10 kHz |
| DC Capacitance | $C$ | 10 mF |
| Leakage Inductance | $L_K$ | 2 uH |
| Nominal Output Power | $P_O$ | 1 KW |

**Table 6.** Simulated and experimental results [10].

| Parameters | Simulated Values | Experimental Values |
|---|---|---|
| Primary Voltage | 13 V (red) | 12 V |
| Secondary Voltage | 270 V (Blue) | 275 V |
| DAB Output Voltage | 286.5 V | 256 V |
| Phase Voltage $V_{P,rms}$ | 118 V | 98 V |
| $THD_V$, | 1.47% | 1.7% |

A total harmonics distortion (THD) value of 1.47% is obtained, as shown in Figure 15, and the output voltage is almost free of harmonics, as presented in Figure 16.

An experimental prototype, shown in Figure 17, is assembled for the validation of the simulation results, as shown in Figures 18–21. Low-voltage MOSFETs, high-voltage IGBTs, and diodes are used in the prototype. The high-frequency transformer is wound on a toroidal core using 10- and 18-gauge wire on the primary and secondary side, respectively. A ferrite core with high permeability up to 1000 is selected to reduce the winding complexity and number of turns. Similarly, the leakage inductance is lower when compared with a core-type or shell-type transformer. The graph shown in Figure 22 depicts the relationship between efficiencies and power output for a variety of loads. $R_L$ = 10–50 ohms when the input voltage $V_{in}$ is 12 V and the output voltage $V_{P,rms}$ is 98 V. It has been realized that the proposed converter has the potential to achieve an efficiency of up to 85%. However, the efficiency can further be increased by increasing the switching frequency, which results in less leakage inductance, and a highly efficient system can be obtained. In [84], a coupled inductor diode-based boost inverter is presented whose results are compared with the proposed topology. The intermediated DC voltage in the proposed topology obtained is 286.5 V, while the DC link voltage of the selected topology for comparison is 600 V. Hence, it resulted in the increased size of the capacitor at the DC link.

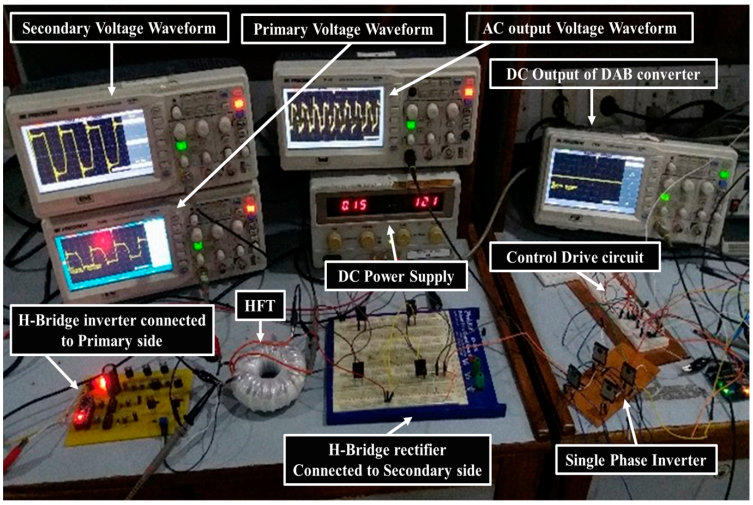


**Figure 17.** Prototype of dual active bridge-based boost inverter.

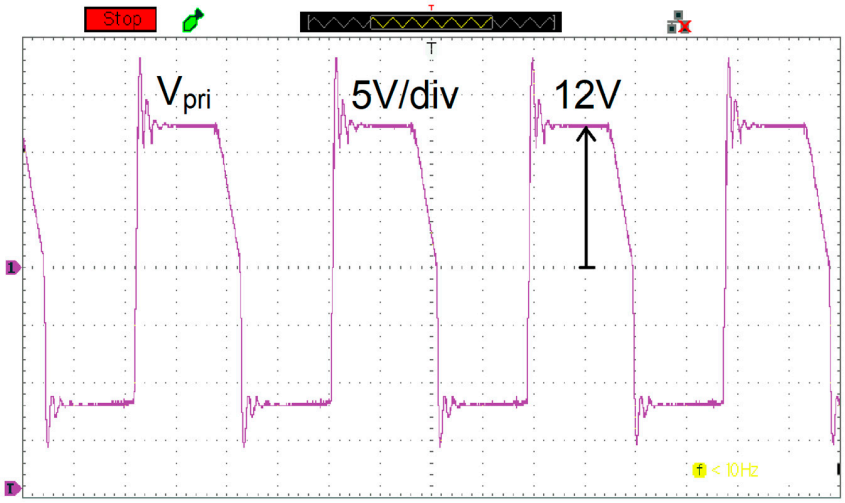


**Figure 18.** Output voltage of H-bridge and input to high-frequency transformer.


**Figure 19.** Secondary voltage of high-frequency transformer.

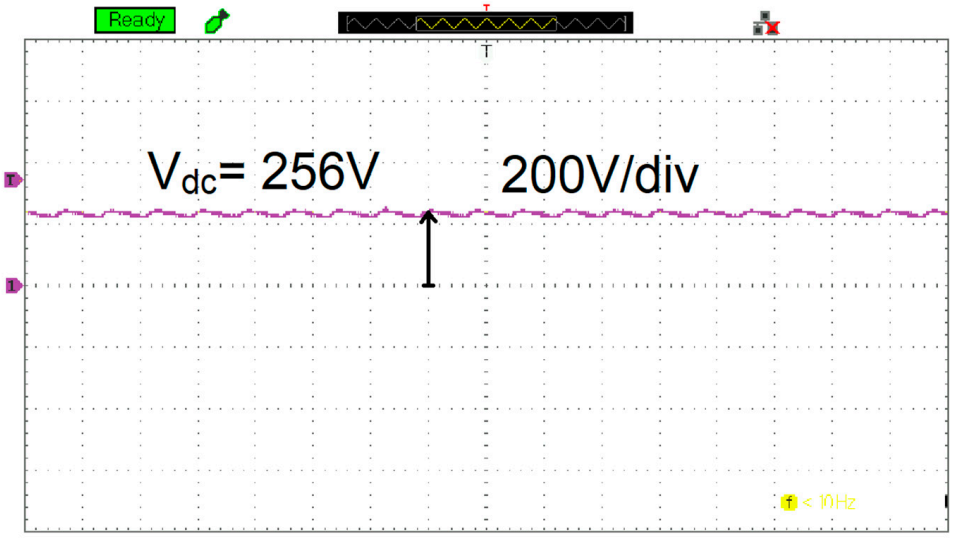


**Figure 20.** Output voltage of DAB converter.

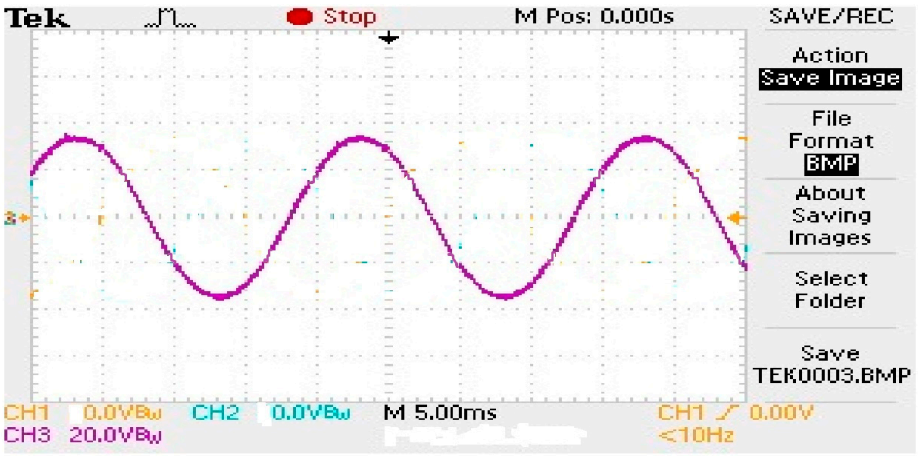


**Figure 21.** Output voltage of dual active bridge-based boost inverter.

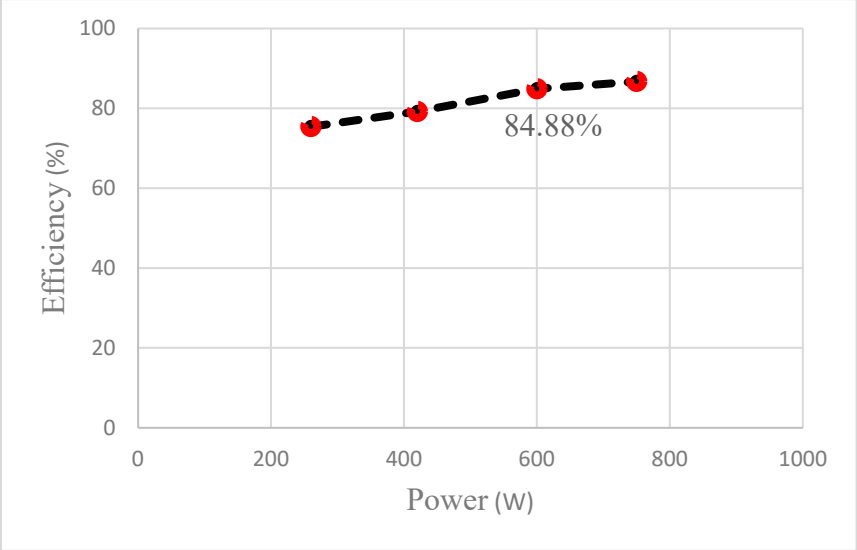


**Figure 22.** Efficiency curve of dual active bridge-based boost inverter.

## 6. Discussion

Several DAB converter topologies have been explored for applications like smart grids, solid state transformers, and uninterrupted power supplies (UPS). The following essential characteristics for future use in various applications should be considered: lesser losses, reduced size, cost-effectiveness, power semiconductor devices exhibiting high temperature characteristics, and DC fault management. Multi-terminal DC systems are considered as future smart grids, including many energy sources [85]. In [86], the authors discuss two excellent topologies, i.e., NPC and DAB. This article discusses only the DAB converter and its topologies. These topologies manage power among three systems: a PV panel, a battery, and a fuel cell.

Similarly, the controllers identified in Section 4 are confined to PI, SMC, and MPC. According to the systematic review, there is an opportunity to apply SMC and other kinds of controllers, which have previously been validated in DAB converters, to PV systems, batteries, and fuel cells to enhance system performance. Furthermore, the sorted literature reveals that a few of the solutions do not make use of the high-frequency transformer's voltage multiplication capability, which is dependent on the core of the transformer and the number of turns. For instance, in [87], the boosting factor provided is two times, which requires a bulky PV array to obtain an output voltage of nearly 600 V; therefore, an HFT with a high turns ratio will facilitate a higher voltage at the output, and a small PV array or single PV module can be interfaced. Similarly, other parasitic parameters of high-frequency transformers such as leakage inductance and parasitic capacitance can further be improved. The transformer design results are based on 10 kHz frequency; however, the transformer can further be operated at much high frequency to reduce the leakage inductance and maximize the power transfer.

The initial control techniques for DAB converter regulation are PI and PID controllers [88]. Those solutions give a comprehensive explanation of the system model and schematic design, but they are not verified in the presence of perturbations. Furthermore, in [89–91], PI and PID controllers must take into account the linearization of the plant model, affecting the controller robustness, and do not often ensure the performance of a system. Another criterion is met in [92], which design nonlinear control techniques. Sliding mode control, in particular, offers robustness and stability against parameter variation, input, and load fluctuations. In [79], the authors have offered MPC solutions, which are established on realistic models that describe the converter over a large operating range. This sort of controller, however, has a significant limitation due to the need for computing resources for the controller to operate, making the controller an expensive solution,

challenging to integrate into embedded systems, and impractical to design using analogue circuits. Finally, only DAB converters in marine and railway applications have used this form of control technique.

## 7. Conclusions

This work reviews DC–DC DAB converters that are used in energy conversion applications. Based on their structures, DAB converters are classified by offering the pros and cons of each kind to identify the appropriate topology. For high voltages, galvanic isolation is necessary because it improves the operation of switching devices and reduces circulating reactive power. The DAB and MMC families are the optimum topologies for bidirectional power flow with galvanic isolation. An MMC combined with a DAB provides the optimum topology for bidirectional power flow with galvanic isolation and enhances the overall efficiency of the system. A high-frequency transformer for a high conversion ratio is discussed in detail, and a toroidal transformer is designed in ANSYS Maxwell with minimum leakage inductance. Although PID controllers are used in DAB converters, it is evident that there is a wide scope to investigate more-sophisticated control approaches that might deliver better outcomes. However, considering the rising demand for renewable energy devices, increasing efficiency is critical in order to offer more power to the load; thus, the DAB converter is employed due to the high efficiency obtainable at high voltage gain compared to standard boost converters. This article compares various control techniques used with DAB-based DC–DC converters, and their advantages and limitations are discussed. DAB converters have a large scope of application in areas such as uninterrupted power supplies, grid-connected renewable energy sources, and marine applications, and they can be extended to solid-state transformers.

**Author Contributions:** Conceptualization, H.A.; investigation, T.I.; methodology, I.U.K.; software, U.A.; writing—original draft, H.A.; writing—review and editing, V.B., L.P. and N.U. All authors have read and agreed to the published version of the manuscript.

**Funding:** This paper was supported by the following projects: The Doctoral Grant Competition VSB—Technical University of Ostrava, reg. no. CZ.02.2.69/0.0/0.0/19 073/0016945 within the Operational Programme Research, Development, and Education, under project DGS/TEAM/2020-017 "Smart Control System for Energy Flow Optimization and Management in a Microgrid with V2H/V2G Technology" and project TN01000007, National Centre for Energy.

**Conflicts of Interest:** The authors declare no conflict of interest.

## References

1. Das, D.; Hrishikesan, V.M.; Kumar, C.; Liserre, M. Smart Transformer-Enabled Meshed Hybrid Distribution Grid. *IEEE Trans. Ind. Electron.* **2020**, *68*, 282–292. [CrossRef]
2. Ruiz, F.; Perez, M.A.; Espinosa, J.R.; Gajowik, T.; Stynski, S.; Malinowski, M. Surveying Solid-State Transformer Structures andControls: Providing Highly Efficient and Controllable Power Flow in Distribution Grids. *IEEE Ind. Electron. Mag.* **2020**, *14*, 56–70. [CrossRef]
3. Liserre, M.; Buticchi, G.; Andresen, M.; De Carne, G.; Costa, L.; Zou, Z.-X. The Smart Transformer: Impact on the Electric Grid and Technology Challenges. *IEEE Ind. Electron. Mag.* **2016**, *10*, 46–58. [CrossRef]
4. Buticchi, G.; Costa, L.F.; Barater, D.; Liserre, M.; Amarillo, E.D. A Quadruple Active Bridge Converter for the Storage Integration on the More Electric Aircraft. *IEEE Trans. Power Electron.* **2017**, *33*, 8174–8186. [CrossRef]
5. Krismer, F.; Kolar, J.W. Accurate power loss model derivation of a high-current dual active bridge converter for an auto-motive application. *IEEE Trans. Ind. Electron.* **2010**, *57*, 881–891. [CrossRef]
6. Shi, Y.; Li, R.; Xue, Y.; Li, H. Optimized Operation of Current-Fed Dual Active Bridge DC–DC Converter for PV Applications. *IEEE Trans. Ind. Electron.* **2015**, *62*, 6986–6995. [CrossRef]
7. Aldosari, O.; Garcia Rodriguez, L.A.; Balda, J.C.; Mazumder, S.K. Design trade-offs for medium- and high-frequency transformers for isolated power converters in distribution system applications. In Proceedings of the 2018 9th IEEE International Symposium on Power Electronics for Distributed Generation Systems (PEDG), Charlotte, NC, USA, 25–28 June 2018; IEEE: Piscataway, NJ, USA, 2018; pp. 1–7.
8. Herrera-Jaramillo, D.A.; Montoya, D.G.; Henao-Bravo, E.E.; Ramos-Paja, C.A.; Saavedra-Montes, A.J. Systematic analysis of control techniques for the dual active bridge converter in photovoltaic applications. *Int. J. Circuit Theory Appl.* **2021**, *49*, 3031–3052. [CrossRef]

9. Du, Y.; Baek, S.; Bhattacharya, S.; Huang, A.Q. High-voltage high-frequency transformer design for a 7.2kV to 120V/240V 20kVA solid state transformer. In Proceedings of the IECON 2010—36th Annual Conference on IEEE Industrial Electronics Society, Glendale, AZ, USA, 7–10 November 2010; pp. 493–498. [CrossRef]
10. Liu, C.; Qi, L.; Cui, X.; Wei, X. Experimental extraction of parasitic capacitances for high-frequency transformers. *IEEE Trans. Power Electron.* **2017**, *32*, 4157–4167. [CrossRef]
11. Ataullah, H.; Iqbal, T.; Khalil, I.U.; Mohammad, A.-S.; Ullah, N.; Emad Farrag, M. Analysis and Verification of Leakage Inductance Calculation in DAB Converters Based on High-Frequency Toroidal Transformers under Different Design Scenarios. *Energies* **2022**, *15*, 6176. [CrossRef]
12. Hazra, S.; Madhusoodhanan, S.; Moghaddam, G.K.; Hatua, K.; Bhattacharya, S. Design considerations and performance evaluation of 1200V 100A sic mosfet-based two-level voltage source converter. *IEEE Trans. Ind Appl.* **2016**, *52*, 4257–4268. [CrossRef]
13. Zhao, B.; Song, Q.; Liu, W.; Sun, Y. Overview of dual-active-bridge isolated bidirectional dc–dc converter for high-frequency-link power conversion system. *IEEE Trans. Power Electron.* **2014**, *29*, 4091–4106. [CrossRef]
14. Zhao, B.; Yu, Q.; Sun, W. Extended-phase-shift control of isolated bidirectional dc-dc converter for power distribution. *IEEE Trans. Power Electron.* **2012**, *27*, 4667–4680. [CrossRef]
15. Bai, H.; Mi, C. Eliminate reactive power and increase system efficiency of isolated bidirectional dual-active-bridge dc–dc converters using novel dual-phase-shift control. *IEEE Trans. Power Electron.* **2008**, *23*, 2905–2914. [CrossRef]
16. Zhao, B.; Song, Q.; Liu, W.; Sun, W. Current-stress-optimized switching strategy of isolated bidirectional dc–dc converter with dualphase-shift control. *IEEE Trans. Ind. Electron.* **2013**, *60*, 4458–4467. [CrossRef]
17. Zhu, L. A novel soft-commutating isolated boost full-bridge ZVSPWM dc–dc converter for bidirectional high power applications. *IEEE Trans. Power Electron.* **2006**, *21*, 422–429. [CrossRef]
18. Madhusoodhanan, S.; Tripathi, A.; Patel, D.; Mainali, K.; Kadavelugu, A.; Hazra, S.; Bhattacharya, S. Solid-state transformer and MV grid tie applications enabled by 15 kV SiC igbts and 10 kV SiC mosfets based multilevel converters. *IEEE Trans. Ind. Appl.* **2015**, *51*, 3343–3360. [CrossRef]
19. De Din, E.; Siddique, H.A.B.; Cupelli, M.; Monti, A.; De Doncker, R.W. Voltage control of parallel-connected dual-active bridge converters for shipboard applications. *IEEE Trans. Emerg. Sel. Topics Power Electron.* **2018**, *6*, 664–673. [CrossRef]
20. Hu, J.; Joebges, P.; Pasupuleti, G.; Averous, N.R. A maximum-output-power-point-tracking-controlled dual active bridge converter for pv energy integration into mvdc grids. *IEEE Trans. Energy Convers.* **2019**, *34*, 170–180. [CrossRef]
21. Liu, P.; Chen, C.; Duan, S. An optimized modulation strategy for the three-level dab converter with five control degrees of freedom. *IEEE Trans. Ind. Electron.* **2020**, *67*, 254–264. [CrossRef]
22. Alhurayyis, I.; Elkhateb, A.; Morrow, D.J. Isolated and non-isolated DC-to-DC converters for medium voltage DC networks: A review. *IEEE J. Emerg. Sel. Top. Power Electron.* **2020**, *9*, 7486–7500. [CrossRef]
23. Dujic, D.; Zhao, C.; Mester, A.; Steinke, J.K.; Weiss, M.; Lewdeni-Schmid, S.; Chaudhuri, T.; Stefanutti, P. Power electronic traction transformer-low voltage prototype. *IEEE Trans. Power Electron.* **2013**, *28*, 5522–5534. [CrossRef]
24. Awal, M.A.; Bipu, R.H.; Montes, O.A.; Feng, H.; Husain, I.; Yu, W.; Lukic, S. Capacitor voltage balancing for neutral point clamped dual active bridge converters. *IEEE Trans. Power Electron.* **2020**, *35*, 11267–11276. [CrossRef]
25. Du, Q.; Gao, L.; Li, Q.; Li, T.; Meng, F. Harmonic reduction methods at DC side of parallel-connected multipulse rectifiers: A review. *IEEE Trans. Power Electron.* **2020**, *36*, 2768–2782. [CrossRef]
26. Filba-Martinez, A.; Busquets-Monge, S.; Bordonau, J. Modulation and capacitor voltage balancing control of multilevel npc dual active bridge DC–DC converters. *IEEE Trans. Ind. Electron.* **2019**, *67*, 2499–2510. [CrossRef]
27. Burkart, R.; Kolar, J. Comparative $\eta$– $\rho$– $\sigma$ pareto optimization of si and sic multilevel dual-active-bridge topologies with wide input. *IEEE Trans. Power Electron.* **2017**, *32*, 5258–5270. [CrossRef]
28. Lee, J.; Choi, H.; Jung, J. Three level npc dual active bridge capacitor voltage balancing switching modulation. In Proceedings of the 2017 IEEE International Telecommunications Energy Conference (INTELEC), Broadbeach, QLD, Australia, 22–26 October 2017; pp. 438–443.
29. Moonem, M.; Duman, T.; Krishnaswami, H. Capacitor voltage balancing in a neutral-point clamped multilevel dc-dc dual active bridge converter. In Proceedings of the 2017 IEEE 8th International Symposium on Power Electronics for Distributed Generation Systems (PEDG), Florianopolis, Brazil, 17–20 April 2017.
30. Feng, H.; Fei, T.; Oscar Andrés, M.; Awal, M.A.; Md Rashed Hassan, B.; Iqbal, H.; Srdjan, L. Passive Capacitor Voltage Balancing of SiC-Based Three-Level Dual-Active-Bridge Converter Using Hybrid NPC-Flying Capacitor Structure. *IEEE Trans. Power Electron.* **2021**, *37*, 4183–4194. [CrossRef]
31. Franquelo, L.G.; Rodriguez, J.; Leon, J.I.; Kouro, S.; Portillo, R.; Prats, M.A. The age of multilevel converters arrives. *IEEE Ind. Electron. Mag.* **2008**, *2*, 28–39. [CrossRef]
32. Liu, Y.; Mao, X.; Ning, G.; Dan, H.; Wang, H.; Su, M. Model predictive-based voltage balancing control for single-phase three-level inverters. *IEEE Trans. Power Electron.* **2021**, *36*, 12177–12182. [CrossRef]
33. Wu, W.; Wang, D.; Liu, L. A multi-layer sequential model predictive control of three-phase two-leg seven-level t-type nested neutral point clamped converter without weighting factors. *IEEE Access* **2019**, *7*, 162735–162746. [CrossRef]
34. Zumel, P.; Ortega, L.; Lazaro, A.; Fernandez, C. Modular dual-active bridge converter architecture. *IEEE Trans. Ind Appl.* **2016**, *52*, 2444–2455. [CrossRef]

35. Shi, Y. Modular Current-Fed Dual-Active-Bridge dc-dc Converters for Medium Voltage System Applications. Ph.D. Thesis, Florida State University, Tallahassee, FL, USA, 2016.
36. Xie, R.; Li, H. Fault performance comparison study of a dual active bridge (dab) converter and an isolated modular multilevel dc/dc (im2dc) converter for power conversion module application in a breaker-less. *IEEE Trans. Ind Appl.* **2018**, *54*, 5444–5455. [CrossRef]
37. Wei, Q.; Wu, B.; Xu, D.; Zargari, N. Model predictive control of capacitor voltage balancing for cascaded modular dc–dc converters. *IEEE Trans. Power Electron.* **2017**, *32*, 752–761. [CrossRef]
38. Si, Y. Advanced Control of Distributed Energy Resource (DER) Inverters and Electric Vehicle (EV) Traction Drives. Ph.D. Thesis, Arizona State University, Tempe, AZ, USA, 2022.
39. Martinez, A.; Monge, S.; Apruzzese, J.; Bordonau, J. Operating principle and performance optimization of a three-level npc dual-active bridge dc–dc converter. *IEEE Trans. Ind. Electron.* **2016**, *63*, 678–690. [CrossRef]
40. Abbasi, M.; Lam, J. A step-up transformerless, zv–zcs high-gain dc/dc converter with output voltage regulation using modular step-up resonant cells for dc grid in wind systems. *IEEE Trans. Emerg. Sel. Topics Power Electron.* **2017**, *5*, 1102–1121. [CrossRef]
41. Dincan, C.; Kjaer, P.; Chen, Y.-H.; Munk-Nielsen, S. Analysis of a high-power, resonant dc–dc converter for dc wind turbines. *IEEE Trans. Power Electron.* **2018**, *33*, 7438–7454. [CrossRef]
42. Cui, S.; Hu, J.; De Doncker, R.W. Control and experiment of a TLC-MMC hybrid DC–DC converter for the interconnection of MVDC and HVDC grids. *IEEE Trans. Power Electron.* **2019**, *35*, 2353–2362. [CrossRef]
43. Faisal, M.; Hannan, M.A.; Ker, P.J.; Hussain, A.; Mansur, M.; Blaabjerg, F. Review of energy storage system technologies in microgrid applications: Issues and challenges. *IEEE Access* **2018**, *6*, 35143–35164. [CrossRef]
44. Huang, S.; Liao, W.; Liu, P.; Tang, W.; Huang, S. Analysis and calculation on switching frequency and switching losses of modular multilevel converter with maximum sub-module capacitor voltage deviation. *IET Power Electron.* **2016**, *9*, 188–197. [CrossRef]
45. Wang, L.; Zhu, Q.; Yu, W.; Huang, A. A medium-voltage medium frequency isolated dc–dc converter based. *IEEE Trans. Emerg. Sel. Topics Power Electron.* **2017**, *5*, 100–109. [CrossRef]
46. Cui, S.; Soltau, N.; de Doncker, R. A high step-up ratio soft switching dc–dc converter for interconnection of mvdc and hvdc grids. *IEEE Trans. Power Electron.* **2018**, *33*, 2986–3001. [CrossRef]
47. Cui, S.; Lee, J.-H.; Hu, J.; De Doncker, R.W.; Sul, S.-K. A modular multilevel converter with a zigzag transformer for bipolar mvdc distribution systems. *IEEE Trans. Power Electron.* **2019**, *34*, 1038–1043. [CrossRef]
48. Shu, L.; Chen, W.; Ning, G.; Cao, W. A resonant zv zcs dc–dc converter with two uneven transformers for an mvdc collection system of offshore wind farms. *IEEE Trans. Ind. Electron.* **2017**, *64*, 7886–7895. [CrossRef]
49. Xiang, X.; Zhang, X.; Chaffey, G.; Green, T. An isolated resonant mode modular converter with flexible modulation and variety of configurations for mvdc application. *IEEE Trans. Power Del.* **2018**, *33*, 508–519. [CrossRef]
50. Hu, Y.; Zeng, R.; Cao, W.; Zhang, J. Design of a modular, high step-up ratio dc–dc converter for hvdc applications integrating offshore wind power. *IEEE Trans. Ind. Electron.* **2016**, *63*, 2190–2202. [CrossRef]
51. Pagliosa, M.; Faust, R.; Lazzarin, T.; Barbi, I. Input-series and output-series connected modular single-switch flyback converter operating in the discontinuous conduction mode. *IET Power Electron.* **2016**, *9*, 1962–1970. [CrossRef]
52. Khalil, I.U.; Ul-Haq, A.; Mahmoud, Y.; Jalal, M.; Aamir, M.; Ahsan, M.U.; Mehmood, K. Comparative analysis of photovoltaic faults and performance evaluation of its detection techniques. *IEEE Access* **2020**, *8*, 26676–26700. [CrossRef]
53. Hou, N.; Song, W.; Wu, M. Minimum-Current-Stress Scheme of Dual Active Bridge DC–DC Converter with Unified Phase-Shift Control. *IEEE Trans. Power Electron.* **2016**, *31*, 8552–8561. [CrossRef]
54. Karthikeyan, V.; Gupta, R. Zero circulating current modulation for isolated bidirectional dual-active-bridge DC–DC converter. *IET Power Electron.* **2016**, *9*, 1553–1561. [CrossRef]
55. Song, W.; Hou, N.; Wu, M. Virtual Direct Power Control Scheme of Dual Active Bridge DC–DC Converters for Fast Dynamic Response. *IEEE Trans. Power Electron.* **2018**, *33*, 1750–1759. [CrossRef]
56. Shi, H.; Wen, H.; Chen, J.; Hu, Y.; Jiang, L.; Chen, G. Minimum Reactive-Power Scheme of Dual-Active-Bridge DC–DC Converter With Three-Level Modulated Phase-Shift Control. *IEEE Trans. Ind. Appl.* **2017**, *53*, 5573–5586. [CrossRef]
57. Das, R.; UddinChowdhury, M.A. PI controlled Bi-directional DC-DC converter (BDDDC) and highly efficient boost converter for electric vehicles. In Proceedings of the 2016 3rd International Conference on Electrical Engineering and Information Communication Technology (ICEEICT), Dhaka, Bangladesh, 22–24 September 2016; IEEE: Piscataway, NJ, USA, 2016.
58. Chauhan, S.; Narsa Reddy, T. High frequency AC Link Based Isolated Dual Active Bridge DC-DC Converter Control, Features and Its Functionalities. In Proceedings of the 2020 IEEE International Conference on Power Electronics, Smart Grid and Renewable Energy (PESGRE2020), Cochin, India, 2–4 January 2020; IEEE: Piscataway, NJ, USA, 2020.
59. Liu, P.; Shanxu, D. A hybrid modulation strategy providing lower inductor current for the DAB converter with the aid of DC blocking capacitors. *IEEE Trans. Power Electron.* **2019**, *35*, 4309–4320. [CrossRef]
60. Coelho, S.; Sousa, T.J.C.; Monteiro, V.; Machado, L.; Afonso, J.L.; Couto, C. Comparative Analysis and Validation of Different Modulation Strategies for an Isolated DC-DC Dual Active Bridge Converter. In Proceedings of the Sustainable Energy for Smart Cities: Second EAI International Conference, SESC 2020, Viana do Castelo, Portugal, 4 December 2020; Springer International Publishing: Berlin/Heidelberg, Germany, 2021.
61. Pan, X.; Yang, F.; Li, L.; Zhang, R.; Wang, C. An Improved Modulation Scheme of Active Commutated Current-Fed Bidirectional dc/dc Converter. *IEEE J. Emerg. Sel. Top. Power Electron.* **2020**, *9*, 1375–1388. [CrossRef]

62. An, F.; Song, W.; Yang, K. Direct power control of dual-active bridge dc–dc converters based on unified phase shift control. *J. Eng.* **2019**, *3*, 2180–2184. [CrossRef]
63. Hua, B.; Chunting, M.; Chongwu, W.; Gargies, S. The dynamic model and hybrid phase-shift control of a dual-active-bridge converter. In Proceedings of the 2008 34th Annual Conference of IEEE Industrial Electronics, Orlando, FL, USA, 10–13 November 2008; IEEE: Piscataway, NJ, USA, 2008; pp. 2840–2845.
64. Qin, H.; Kimball, J.W. *Closed-Loop Control of DC–DC Dual Active Bridge Converters Driving Single-Phase Inverters*; IEEE: Piscataway, NJ, USA, 2012; pp. 173–179.
65. Syed, I.; Xiao, W. Modeling and control of DAB applied in a PV based DC microgrid. In Proceedings of the 2012 IEEE International Conference on Power Electronics, Drives and Energy Systems (PEDES), Bengaluru, India, 16–19 December 2012; IEEE: Piscataway, NJ, USA, 2012; pp. 1–6.
66. Everts, J.; Everts, J. Design and optimization of an efficient (96.1%) and compact (2 kW/dm3) bidirectional isolated single-phase dual active bridge AC–DC converter. *Energies* **2016**, *9*, 799. [CrossRef]
67. You, J.; Xia, J.; Jia, H. Analysis and control of DAB based DC–AC multiport converter with small DC link capacitor. In Proceedings of the IECON 2017-43rd Annual Conference of the IEEE Industrial Electronics Society, Beijing, China, 29 October–1 November 2017; IEEE: Piscataway, NJ, USA, 2017; pp. 823–828.
68. Lemus, J.; Vélez, G.C.; Rodrıguez, N.J.C. Pid controller design for dc motor. *Contemp. Eng. Sci.* **2018**, *11*, 4913–4920. [CrossRef]
69. Khan, M.R.; Khan, A.A.; Ghazali, U. Speed Control of DC Motor under Varying Load Using PID Controller. *Int. J. Eng.* **2015**, *9*, 38–48.
70. Ramya, K.; Jegathesan, V. Comparison of pi and pid controlled bidirectional dc-dc converter systems. *Int. J. Power Electron. Drive Syst.* **2016**, *7*, 56. [CrossRef]
71. Filsoof, K.; Lehn, P.W. A bidirectional multiple-input multiple-output modular multilevel DC–DC converter and its control design. *IEEE Trans Power Electron.* **2015**, *31*, 2767–2779. [CrossRef]
72. Ali, M.; Aamir, M.; Khan, H.S.; Khan, A.A.; Haroon, F. Design and Implementation of Fractional-Order Sliding Mode Control for Parallel Distributed Generations Units in Islanded Microgrid. In Proceedings of the IEEE 28th International Symposium on Industrial Electronics (ISIE), Vancouver, BC, Canada, 12–14 June 2019; IEEE: Piscataway, NJ, USA, 2019; pp. 64–69.
73. Jeung, Y.-C.; Choi, I.-C.; Lee, D.-C. Robust voltage control of dual active bridge DC-DC converters using sliding mode control. In Proceedings of the IEEE 8th International Power Electronics and Motion Control Conference (IPEMC-ECCE Asia), Hefei, China, 22–26 May 2016; IEEE: Piscataway, NJ, USA, 2016.
74. Jeung, Y.-C.; Dong-Choon, L. Voltage and current regulations of bidirectional isolated dual-active-bridge DC–DC converters based on a double-integral sliding mode control. *IEEE Trans. Power Electron.* **2018**, *34*, 6937–6946. [CrossRef]
75. Talbi, S.; Mabwe, A.M.; Hajjaji, A.E. Control of a bidirectional dual active bridge converter for charge and discharge of a Li-ion battery. In Proceedings of the IECON 2015-41st Annual Conference of the IEEE Industrial Electronics Society, Yokohama, Japan, 9–12 November 2015; IEEE: Piscataway, NJ, USA, 2015; pp. 849–856.
76. Frances, A.; Asensi, R.; García, Ó.; Prieto, R.; Uceda, J. Modeling electronic power converters in smart DC microgrids—An overview. *IEEE Trans. Smart Grid* **2017**, *9*, 6274–6287. [CrossRef]
77. Lee, S.; Jeung, Y.C.; Lee, D.C. Output voltage regulation of IPOS modular dual active bridge DC/DC converters using sliding mode control. In Proceedings of the 2018 IEEE Applied Power Electronics Conference and Exposition (APEC), San Antonio, TX, USA, 4–8 March 2018; IEEE: Piscataway, NJ, USA, 2018; pp. 3062–3067.
78. Kayaalp, R.İ.; Demirdelen, T.; Tümay, M. A novel fuzzy logic control for bidirectional DC-DC converter and comparison with dual phase-shift control method in medium voltage applications. In Proceedings of the 2016 IEEE International Conference on Computational Intelligence and Virtual Environments for Measurement Systems and Applications (CIVEMSA), Budapest, Hungary, 27–28 June 2016; IEEE: Piscataway, NJ, USA, 2016.
79. Cupelli, M.; Gurumurthy, S.K.; Monti, A. Modelling and control of single phase DAB based MVDC shipboard power system. In Proceedings of the IECON 2017-43rd Annual Conference of the IEEE Industrial Electronics Society, Beijing, China, 29 October–1 November 2017; IEEE: Piscataway, NJ, USA, 2017; pp. 6813–6819.
80. An, F.; Song, W.; Yu, B.; Yang, K. Model predictive control with power self-balancing of the output parallel DAB DC–DC converters in power electronic traction transformer. *IEEE J. Emerg. Sel. Top Power Electron.* **2018**, *6*, 1806–1818. [CrossRef]
81. Chen, L.; Shao, S.; Xiao, Q.; Tarisciotti, L.; Dragicevic, T.; Wheeler, P. Model-predictive-control for dual-active-bridge converters supplying pulsed power loads in naval DC microgrids. *IEEE Trans. Power Electron.* **2019**, *35*, 1957–1966. [CrossRef]
82. Bambang, R.T.; Rohman, A.S.; Dronkers, C.J.; Ortega, R.; Sasongko, A. Energy management of fuel cell/battery/supercapacitor hybrid power sources using model predictive control. *IEEE Trans. Ind. Inform.* **2014**, *10*, 1992–2002.
83. Akter, P.; Uddin, M.; Mekhilef, S.; Tan, N.M.L.; Akagi, H. Model predictive control of bidirectional isolated DC–DC converter for energy conversion system. *Int. J. Electron.* **2015**, *102*, 1407–1427. [CrossRef]
84. Iqbal, T.; Lu, H.; Zaman, S.; Tan, S.C.; Li, G.; Zhang, X. Coupled-inductor based diode assisted boost inverter for achieving highgain. *IET Power Electron.* **2019**, *12*, 410–420. [CrossRef]
85. Kish, G. On the emerging class of non-isolated modular multilevel dc–dc converters for dc and hybrid ac–dc systems. *IEEE Trans. Smart Grid.* **2019**, *10*, 1762–1771. [CrossRef]
86. Kolahian, P.; Tarzamni, H.; Nikafrooz, A.; Hamzeh, M. Multi-port dc–dc converter for bipolar medium voltage dc micro-grid applications. *IET Power Electron.* **2019**, *12*, 1841–1849. [CrossRef]

87. Shi, Y.; Li, R.; Xue, Y.; Li, H. High-frequency-link-based grid-tied PV system with small DC-link capacitor and low-frequency ripple-free maximum power point tracking. *IEEE Trans. Power Electron.* **2016**, *31*, 328–339. [CrossRef]
88. Koch, G.G.; Queiroz, S.S.; Rech, C.; Oliveira, R.C.; Borges, R.A.; Tognetti, E.S.; Montagner, V.F. Design of a robust PI controller for a dual active bridge converter. In Proceedings of the 2016 12th IEEE International Conference on Industry Applications (INDUSCON), Curitiba, Brazil, 20–23 November 2016; pp. 1–6.
89. Hu, J.; Joebges, P.; De Doncker, R.W. *Maximum Power Point Tracking Control of a High Power DC–DC Converter for PV Integration in MVDC Distribution Grids*; Institute for Power Generation and Storage Systems, E. on Energy Research Center, RWTH Aachen University: Aachen, Germany, 2017; pp. 1259–1266.
90. Öztürk, S.; Pos¸pos¸, P.; Utalay, V.; Koç, A.; Ermis, M.; Çadırcı, I. Operating principles and practical design aspects of all SiC DC/AC/DC converter for MPPT in grid-connected PV supplies. *Sol. Energy* **2018**, *176*, 380–394. [CrossRef]
91. Duman, T.; Marti, S.; Moonem, M.A.; Kader, A.A.R.A.; Krishnaswami, H. A modular multilevel converter with power mismatch control for grid-connected photovoltaic systems. *Energies* **2017**, *10*, 698. [CrossRef]
92. Gonzales, O.; Rosales, A. Sliding mode controller based on a linear quadratic integral regulator surface for power control on a dual active bridge converter. In Proceedings of the 2018 IEEE Third Ecuador Technical Chapters Meeting (ETCM), Cuenca, Ecuador, 15–19 October 2018; IEEE: Piscataway, NJ, USA, 2018; pp. 1–6.